Astron. Astrophys. 348, 286–294 (1999)

ASTRONOMY
AND
ASTROPHYSICS

The absolute coronal abundances of sulfur, calcium, and iron from Yohkoh-BCS flare spectra

A. Fludra[1] **and J.T. Schmelz**[2]

[1] Space Science Department, Rutherford Appleton Laboratory, Chilton, Didcot, OX11 0QX, UK (A.Fludra@rl.ac.uk)
[2] Physics Department, University of Memphis, Memphis, TN 38152, USA

Received 1 April 1999 / Accepted 5 May 1999

Abstract. Using X-ray spectra from the Bragg Crystal Spectrometer on *Yohkoh*, we have derived the absolute coronal abundances of sulfur, calcium, and iron using the ratio of the flux in the S XV, Ca XIX and Fe XXV resonance lines to the continuum near the Ca XIX and S XV resonance lines. For the 57 flares analyzed here, multi-thermal effects have been taken into account using a differential emission measure analysis. We compare these abundances of S, Ca, and Fe with their photospheric values and with values derived for coronal plasma from both spectral and solar energetic particle data. The mean *Yohkoh* abundance of sulfur relative to hydrogen is 7.9×10^{-6}, smaller than the photospheric value by over a factor of two. The mean abundance of calcium is 3.4×10^{-6}, about 50% greater than the photospheric value. The mean abundance of iron shows greater scatter around its mean value of 4.5×10^{-5}, but is still higher than the accepted photospheric value. Comparison of these results with others already in the literature, suggests that the coronal abundance-normalization problem does not have a simple solution.

Key words: Sun: abundances – Sun: corona – Sun: flares – Sun: X-rays, gamma rays

1. Introduction

Knowledge of abundances of trace elements relative to hydrogen (i.e., absolute abundances) in solar coronal plasma is essential for the analysis of plasma conditions. The last two decades have brought the discovery that the coronal abundances are different from photospheric abundances. Both spectroscopic and solar energetic particle (SEP) data agree that the coronal-to-photospheric abundance ratios of elements with low First Ionization Potential (FIP $<$10 eV) seem to be enhanced by about a factor of four relative to those with high FIP ($>$11 eV). This fractionation probably results from a separation of ions and neutrals, which takes place at temperatures between 6000 and 10,000 K. Modeling of the abundances of solar coronal plasma has indeed shown that the coronal abundances may be made to differ from their photospheric counterparts by invoking a mechanism which depends on the FIP of the element and which separates the ions from the neutral atoms, and feeds the modified mixture upwards into coronal loops.

The observations, however, are not unequivocal on the normalization of the trace elements *with respect to hydrogen*, a result which is problematic in both the spectroscopic and SEP data analysis. Two different empirical models have been suggested in the literature: (1) low-FIP elements may be enhanced by about a factor of four with respect to their photospheric values while high-FIP elements are the same in the corona and the photosphere (Feldman 1992; Meyer 1993) or (2) low-FIP elements may be the same in the corona and the photosphere while high-FIP elements are depleted by about a factor of four with respect to their photospheric values (Meyer 1985, 1991). The data that support model (1) are mainly the SEP results presented by Reames (1995) and partially the Ca/H spectroscopic results first presented by Sylwester et al. (1984), Lemen et al. (1986), and Sylwester et al. (1998). Model (2) was originally proposed based on the spectroscopic results of Veck & Parkinson (1981), and later appeared consistent with other spectroscopic measurements by Fludra et al. (1993), Fludra & Schmelz (1995), and Raymond et al. (1997).

The different normalizations suggested by the two different kinds of data may represent physical differences: SEP observations give abundances in plasma that has escaped from the corona and traveled to the vicinity of Earth, while spectroscopic observations measure plasma that remains confined in coronal loops. Therefore, SEP and spectroscopic observations may correspond to different types of events or different parts of the corona. Alternatively, the mechanism that accelerates SEPs may be selective.

To date, the observational data cannot conclusively distinguish between version (1) enhanced low FIP elements and version (2) depleted high FIP elements, while the recent theoretical modeling favors option (1). It is possible, however, that neither of these is correct and that some combination of both models gives a more accurate picture of the plasma, where there is both low-FIP enhancement as well as high-FIP depletion, but neither by as great as a factor of four. It is also possible that different normalizations apply under different physical conditions (i.e., different flares or different active regions). We discuss such a hybrid model in this paper.

Send offprint requests to: A. Fludra

Deriving absolute coronal abundances of elements heavier than helium from spectroscopic observations requires measurements of the continuum emission as well as the spectral lines. So far, only three X-ray spectrometers have had the capability to measure the uncontaminated continuum emission: a graphite crystal spectrometer on OSO-8, the Bent Crystal Spectrometer on the Solar Maximum Mission (SMM) and the Bragg Crystal Spectrometer (BCS) on *Yohkoh*. The OSO-8 data analyzed by Veck & Parkinson (1981) provided absolute abundances of silicon, sulfur, calcium and argon. The SMM data gave absolute abundances of calcium (Lemen et al. 1986; Sylwester et al. 1998), calcium and iron (Fludra et al. 1991), and magnesium, oxygen and neon (Fludra & Schmelz 1995). The SMM results and their comparison with SEP and gamma-ray observations are reviewed by Fludra et al. (1999). *Yohkoh*-BCS data were used by Fludra et al. (1993) to derive the sulfur, calcium, and iron abundances for several flares. In this paper, we extend this analysis and derive the abundances of S, Ca, and Fe with respect to hydrogen for 57 flares observed with the BCS. We apply a method of multi-thermal analysis that is a significant departure from a simple line-to-continuum method applied to Ca XIX spectra by, e.g., Sylwester et al. (1998), and allows us to simultaneously derive the absolute abundances of several elements. Sect. 2 describes the data, the method is described in Sect. 3 and the results are given in Sect. 4.

2. Observations

The BCS (Culhane et al. 1991) has a full-Sun field-of-view and observes high temperature, mainly flaring coronal plasma. The instrument has four high spectral resolution channels which register the resonance and satellite lines of S XIV−XV, Ca XVIII−XIX, Fe XXIII−XXV, and Fe XXVI. The spectra are observed with curved germanium crystals and a one-dimensional, position-sensitive proportional counter. The BCS spectra provide information on electron temperature and relative abundances from line flux ratios, line broadening and plasma dynamics from line profiles, and emission measure from line intensities. In addition, the abundances of sulfur, calcium, and iron relative to hydrogen can be estimated from the intensity ratio of the line to continuum. This is possible since the continuum to the left of the resonance lines ($^1S_0 - ^1P_1$) of S XV and Ca XIX, at 5.039 Å and 3.178 Å, respectively, is uncontaminated with line emission and the fluorescence from Ge crystals is electronically separated and rejected.

In this paper we have examined selected time intervals from the 57 BCS flares listed in Table 1. Column (1) lists the flare number, (2) the date of the observation, (3) the flare peak time, (4) the Yohkoh orbit start time, (5) the average derived sulfur abundance, (6) the uncertainty in the sulfur abundance, (7) the average calcium abundance, (8) the uncertainty in the calcium abundance, (9) the average iron abundance, and (10) the uncertainty in the iron abundance. Fig. 1 shows an example of a light curve for the calcium channel for the flare which occurred on 1992 July 17 at 22:35 UT. In general, we concentrate on the peak and decay phase of these flares where conditions are not quite as dynamic as in the rise phase, where there are no evident asymmetries in line profiles indicating plasma upflows, and where the effects of non-equilibrium ionization or non-Maxwellian electron energy distributions should be small. The spectra were integrated for 20–60s time intervals, and several spectra were analyzed for each flare. The temperatures derived independently from sulfur, calcium, and iron spectra were different, indicating a broad distribution of emission measure with temperature. Therefore, to determine the abundances correctly, the multi-temperature effects have been taken into account using the differential emission measure (DEM) calculation described in Sect. 3.2 below.

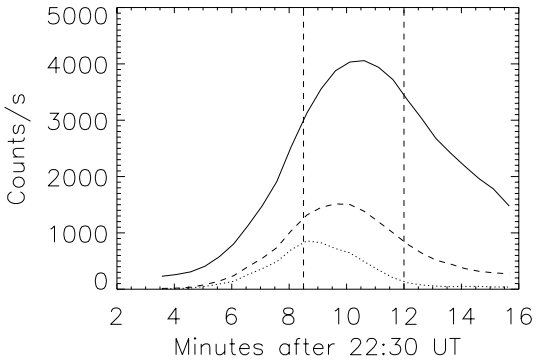

Fig. 1. Example of light curves for the BCS channels for the 1992 July 17, 22:35 UT flare: S XV (solid line), Ca XIX (dashed line), Fe XXV (dotted line). Vertical lines show the time period where the abundances were determined. The spectra were typically integrated for 20–60s time intervals to ensure a good signal to noise ratio, and several spectra were analyzed for each flare.

3. Analysis

3.1. Spectral fitting

The BCS spectra were fitted by calculating a full theoretical spectrum, including the effects of the numerous dielectronic and inner-shell excitation lines, in order to estimate properly the intensity of the resonance line (Fludra et al. 1995). In sulfur spectra (Fig. 2c), the temperature is estimated from the intensity ratio of the lines $k + j + z$ to the resonance line w. The x, y lines are intercombination transitions ($1s^2\ ^1S - 1s2p\ ^3P_2$) and ($1s^2\ ^1S - 1s2p\ ^3P_1$), z is the forbidden transition ($1s^2\ ^1S - 1s2s\ ^3S$) and is blended with the $n = 2$ dielectronic satellites k and j. Therefore, a full spectral fitting is required to derive the temperature. The electron temperature in the calcium spectra (Fig. 2b) is estimated from the ratio of the $n = 3$ dielectronic satellites to the resonance line w. For the Fe XXV spectra (Fig. 2a), the temperature is determined from the ratio of the dielectronic satellite j to the resonance line w. Other lines in the Fe XXIII-XXV theoretical spectrum are calculated from their theoretical data using the temperature from the j/w ratio, however, only spectral pixels around the resonance line and the j line are actually used in the fitting. Fe XXIII lines at wavelengths above 1.870 Å (Lemen et al. 1984) are not fitted. Therefore, the systematic discrepancy between the observed and theoret-

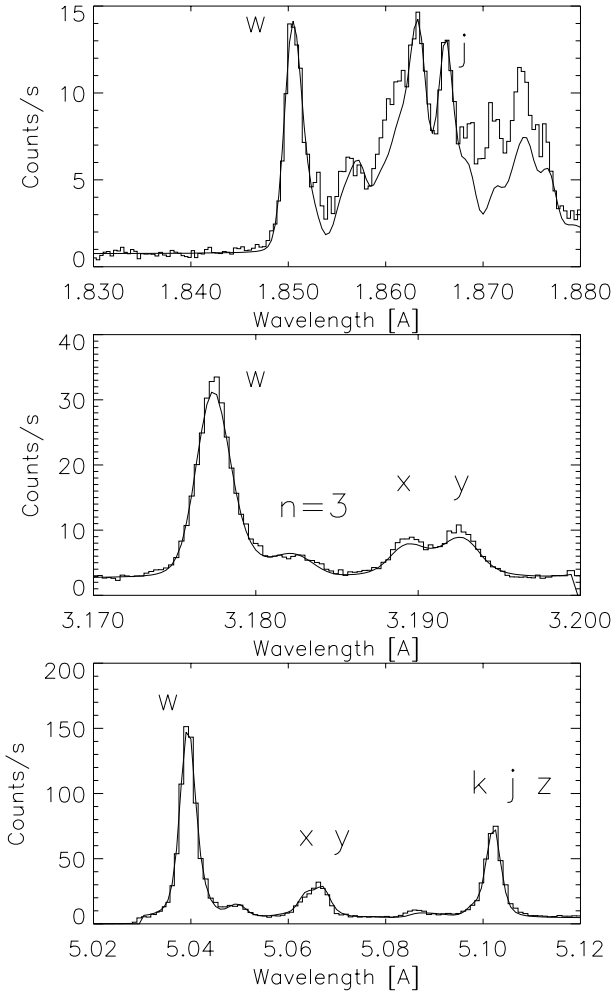

Fig. 2a–c. A 30s spectrum (histogram) for the 1992 July 17 flare observed at 22:39:07 UT in **a** Fe XXIII−XXV with BCS channel 2 (*top panel*), **b** Ca XVIII−XIX with the BCS channel 3 (*middle panel*), and **c** S XIV−XV with the BCS channel 4 (*bottom panel*). The continuous line represents a fitted theoretical spectrum (see Sect. 3.1).

ical spectrum for wavelengths above 1.870 Å seen in Fig. 2a, while indicative of inaccuracies in either the ionization balance calculations or atomic data for those lines, does not affect the temperature determinations.

In all spectra, the numerous dielectronic and inner-shell excitation lines have been included, in order to estimate correctly the intensity of the resonance lines (labeled w in Fig. 2). The synthesized spectra are then convolved with the crystal rocking curve (assumed Lorentzian) and the detector position resolution including electronic noise (assumed Gaussian). The convolved spectrum is compared to the observed spectrum by computing the statistic χ^2. All free parameters are adjusted simultaneously to minimize χ^2, using a gradient search and parabolic expansion algorithm. The fitted parameters are the electron temperature, emission measure, and line width. The statistical uncertainties of the fitted parameters are determined by an algorithm included in the fitting procedure and are interpreted as "one sigma" statistical errors. Details of this fitting method are given by Fludra et al. (1989, 1995).

The atomic data for Ca XIX and Fe XXV are from Bely-Dubau et al. (1982a, b). For S XV spectra the following data are used: wavelengths and atomic data for $n \geq 3$ dielectronic satellites from Dubau (1992), wavelengths for $n = 2$ satellites from Vainshtein & Safronova (1978), the ratios of the intercombination and forbidden lines to the resonance line from McCann & Keenan (1988), and the wavelengths of the w, x, y and z lines from Vainshtein & Safronova (1985). The plasma is assumed to be in ionization equilibrium and the ionization balance calculations by Arnaud & Rothenflug (1985) are used. The line emissivities for all the lines used in this analysis are shown in Fludra et al. (1995).

Fig. 2 shows examples of the spectra and the results of the spectral fitting for the sulfur, calcium, and iron channels for the 1992 July 17 flare. The histogram is the observed spectrum and the solid curve is a theoretical spectrum based on the best fit to selected lines. The temperatures derived for each channel in the example given in Fig. 2 are 12.1 ± 0.6, 13.3 ± 0.4, and 15.5 ± 0.3 MK for sulfur, calcium, and iron. The increase in derived temperature from lines with increasing peak formation temperature – from S XV to Ca XIX and Fe XXV spectra – is typical for all flares. This is indicative of the presence of multithermal plasmas.

Derivation of absolute abundances requires relating the line intensity to the intensity of the continuum. When both the line and the continuum have similar temperature dependence, as is the case with the Ca XIX resonance line and the continuum near this line, the assumption of isothermal plasma is sufficient for the abundance analysis (e.g., Sylwester et al. 1998). However, the temperature dependence of the Fe XXV lines is significantly different from that of the Ca XIX continuum, and to relate the intensities of Fe XXV lines to the Ca XIX continuum it is necessary to take into account the temperature distribution of the plasma. This requires a method that will do the analysis in two stages: first, the DEM (see Sect. 3.2) has to be derived from line intensities without assuming a value for the element's abundance, then the abundances can be derived from line intensities and the DEM. We will use a method introduced by Fludra et al. (1993, 1995) and Fludra & Schmelz (1995), as described below.

3.2. Abundance determination

The flux, F, of an optically thin soft X-ray emission line is given by:

$$F = constant \times A \int G(T)\phi(T)dT \qquad (1)$$

where F is the flux measured at Earth in units of photon s^{-1} cm^{-2}, A is the abundance relative to hydrogen of the element forming the line, $G(T)$ is the emissivity function (a temperature dependent term depending on the excitation and ionization properties of the atom producing the line), and $\phi(T)$ is the DEM, i.e., emission measure between T and $T + dT$.

Table 1. Absolute abundances of S, Ca and Fe in flares observed by Yohkoh-BCS

No.	Date	Peak Time	Orbit Time	Sulfur Abundance	Sulfur Uncertainty	Calcium Abundance	Calcium Uncertainty	Iron Abundance	Iron Uncertainty
1	07-Oct-91	10:18	09:27	7.70E-06	7.1E-07	3.11E-06	4.8E-07	4.66E-05	6.9E-06
2	26-Oct-91	00:12	00:02	7.52E-06	4.4E-07	3.41E-06	2.0E-07	3.44E-05	5.1E-06
3	26-Oct-91	00:40	01:40	7.50E-06	6.4E-07	3.21E-06	3.0E-07		
4	29-Oct-91	19:28	19:17	8.27E-06	2.5E-07	3.09E-06	1.3E-07	4.81E-05	6.1E-06
5	30-Oct-91	19:50	19:43	5.37E-06	4.0E-07	3.99E-06	5.8E-07	5.00E-05	3.6E-06
6	30-Oct-91	20:22	19:43	5.91E-06	8.5E-07	3.13E-06	2.6E-07	4.32E-05	9.2E-06
7	31-Oct-91	09:10	08:45	8.36E-06	1.2E-06	3.28E-06	4.7E-07	3.98E-05	2.5E-06
8	19-Nov-91	09:30	09:29	6.93E-06	8.5E-07	3.33E-06	2.2E-07	2.82E-05	7.1E-06
9	19-Nov-91	19:24	18:30	8.09E-06	7.3E-07	3.81E-06	4.1E-07	3.03E-05	2.7E-06
10	16-Dec-91	22:07	21:54	8.32E-06	5.6E-07	3.44E-06	4.7E-07	4.04E-05	8.4E-06
11	27-Dec-91	06:12	05:21	9.68E-06	1.2E-06	3.63E-06	1.8E-07	3.82E-05	4.3E-06
12	14-Jan-92	19:38	19:20	9.94E-06	9.2E-07	3.24E-06	1.4E-07	4.17E-05	7.5E-06
13	06-Feb-92	10:10	11:01	6.61E-06	4.4E-07	3.46E-06	4.4E-07		
14	21-Feb-92	03:30	02:25	5.83E-06	5.3E-07	4.62E-06	3.2E-07	3.95E-05	4.6E-06
15	21-Feb-92	03:30	04:02	5.90E-06	2.4E-07	3.94E-06	4.2E-07		
16	25-Feb-92	23:33[a]	00:46	9.11E-06	1.8E-07	3.67E-06	1.5E-07		
17	27-Feb-92	09:54	12:57	8.28E-06	5.7E-07	2.74E-06	4.6E-07		
18	01-Apr-92	17:40	18:01	5.84E-06	2.0E-07	3.10E-06	2.1E-07		
19	13-Jul-92	09:29	09:15	8.72E-06	8.5E-07	2.71E-06	2.3E-07		
20	14-Jul-92	10:20	09:36	7.04E-06	3.9E-07	3.49E-06	2.3E-07		
21	14-Jul-92	17:50	17:44	9.28E-06	1.7E-06	3.38E-06	5.1E-07	3.65E-05	6.4E-06
22	15-Jul-92	02:00	01:51	8.78E-06	1.3E-06	3.00E-06	2.7E-07	3.30E-05	1.2E-05
23	15-Jul-92	03:50	03:28	5.73E-06	6.8E-07	2.76E-06	1.5E-07		
24	15-Jul-92	10:51	09:58	9.82E-06	8.7E-07	2.87E-06	2.0E-07	3.45E-05	8.4E-06
25	16-Jul-92	01:10	00:35	8.36E-06	1.2E-06	2.70E-06	2.8E-07	3.77E-05	8.4E-06
26	16-Jul-92	23:58	23:19	1.01E-05	4.8E-07	2.99E-06	1.8E-07	4.67E-05	1.1E-05
27	17-Jul-92	21:10	20:26	1.01E-05	4.8E-07	3.15E-06	2.6E-07	4.07E-05	6.3E-06
28	17-Jul-92	22:40	22:03	9.19E-06	7.9E-07	3.45E-06	4.2E-07	3.88E-05	1.0E-05
29	18-Jul-92	01:38	01:18	9.18E-06	1.2E-06	2.87E-06	2.3E-07	4.27E-05	8.9E-06
30	18-Jul-92	05:10	04:33	1.09E-05	9.3E-07	2.38E-06	2.0E-07		
31	18-Jul-92	13:42	12:40	7.85E-06	4.1E-07	3.63E-06	1.3E-07	5.35E-05	4.5E-06
32	03-Aug-92	06:36	05:43	8.88E-06	1.0E-06	3.52E-06	4.7E-07	4.72E-05	9.5E-06
33	03-Aug-92	07:04	07:20	8.96E-06	3.1E-07	2.64E-06	2.0E-07		
34	03-Aug-92	07:04	08:58	9.01E-06	5.6E-07	2.94E-06	1.3E-07		
35	11-Aug-92	22:26	21:36	7.35E-06	4.4E-07	4.72E-06	4.3E-07	9.06E-05	1.6E-05
36	16-Aug-92	13:58	13:40	5.85E-06	4.5E-07	3.72E-06	3.1E-07	5.09E-05	1.1E-05
37	19-Aug-92	20:10	19:38	7.68E-06	2.9E-07	3.71E-06	2.4E-07	4.43E-05	6.5E-06
38	20-Aug-92	22:08	21:38	7.20E-06	9.1E-07	3.36E-06	2.9E-07		
39	21-Aug-92	06:02	05:45	5.62E-06	4.7E-07	3.68E-06	1.8E-07		

Following Withbroe (1975), $\phi(T)dT = n_e^2 dV$, where n_e is the electron density in cm^{-3}, and V is the volume in cm^3.

Typical DEM techniques solve N linear equations (1). This approach has been modified to take advantage of the BCS continuum measurements and to calculate the abundances of sulfur, calcium, and iron with respect to hydrogen (Fludra et al. 1993, 1995; Fludra & Schmelz 1995). The method requires flux ratios F_{m1}/F_{m2} for K pairs of lines (m1,m2) from the same element. We then solve $L = N - 2K$ linear equations of type Eq. (1) above and K non-linear equations of the type:

$$\frac{F_{m1}}{F_{m2}} = R_m = \frac{\int G_{m1}(T)\phi(T)dT}{\int G_{m2}(T)\phi(T)dT} \quad (2)$$

by minimizing

$$\chi^2(\phi) = \sum_{i=1}^{L} \frac{1}{\sigma_i^2}(F_{i\ obs} - F_{i\ pred})^2 + \sum_{m=1}^{K} \frac{1}{\sigma_m^2}(R_{m\ obs} - R_{m\ pred})^2 \quad (3)$$

where σ is the statistical error. The minimum of χ^2 is found using a Conjugate Gradient technique with a positivity constraint $\phi \geq 0$ (Fludra & Sylwester 1986). The abundance of the element producing line m can then be calculated using

$$A_m = \frac{F_{m\ obs}}{\int G_m(T)\phi(T)dT} \quad (4)$$

Here, we use this technique with the lines observed by the BCS. The three ratios S $(k+j+z)/w$, Ca $(n=3)/w$, and

Table 1. (continued)

No.	Date	Peak Time	Orbit Time	Sulfur Abundance	Sulfur Uncertainty	Calcium Abundance	Calcium Uncertainty	Iron Abundance	Iron Uncertainty
40	21-Aug-92	09:31	09:00	6.60E-06	4.9E-07	4.17E-06	3.9E-07		
41	21-Aug-92	11:09	10:33	7.87E-06	5.1E-07	4.06E-06	2.4E-07	5.59E-05	1.7E-05
42	22-Aug-92	14:51	14:14	7.99E-06	1.1E-06	4.14E-06	4.5E-07	7.67E-05	9.5E-06
43	06-Sep-92	02:11	01:47	9.16E-06	1.1E-06	2.55E-06	3.2E-07	3.00E-05	1.0E-05
44	06-Sep-92	16:45	16:24	6.27E-06	9.8E-07	2.69E-06	2.5E-07	3.14E-05	5.3E-06
45	12-Sep-92	15:40	15:21	5.78E-06	6.0E-07	3.98E-06	2.8E-07	4.76E-05	1.1E-05
46	13-Sep-92	03:03	02:43	5.86E-06	9.7E-07	4.30E-06	1.1E-07		
47	16-Sep-92	23:50	23:20	8.50E-06	1.1E-06	4.10E-06	2.5E-07	6.40E-05	9.3E-06
48	17-Sep-92	10:06	09:05	7.74E-06	5.8E-07	3.40E-06	5.4E-07		
49	17-Sep-92	13:00	12:20	8.16E-06	3.2E-07	3.20E-06	6.2E-08	3.61E-05	6.5E-06
50	17-Sep-92	17:20	17:12	6.61E-06	5.9E-07	3.53E-06	3.1E-07		
51	17-Sep-92	20:50	20:27	8.12E-06	2.9E-07	3.26E-06	3.3E-07	5.77E-05	8.3E-06
52	07-Oct-92	10:11	09:47	1.01E-05	1.4E-06	2.69E-06	2.5E-07	3.24E-05	5.5E-06
53	07-Oct-92	15:02	14:39	9.49E-06	8.3E-07	2.84E-06	5.8E-07		
54	08-Oct-92	02:39	02:01	8.31E-06	8.0E-07	3.06E-06	5.0E-07	2.97E-05	7.6E-06
55	08-Oct-92	04:31	03:39	8.95E-06	4.5E-07	4.22E-06	2.5E-07	5.88E-05	1.1E-05
56	06-Mar-93	20:40	20:34	8.31E-06	2.3E-07	3.17E-06	1.3E-07	4.12E-05	1.0E-05
57	06-Mar-93	22:28	22:12	8.02E-06	2.9E-07	2.80E-06	1.0E-07	5.77E-05	4.7E-06

[a] 23:33 UT on 24-Feb-92

Fe j/w, correspond to Eq. (2) and are used in the second summation of Eq. (3), where $K = 3$. In addition, we include the flux of the continuum measured on the short wavelength side (3.170–3.174 Å) of the Ca XIX resonance line, and the continuum in the S XV spectrum, as the first summation of Eq. (3), with $L = 2$. Thus, the scaling of the differential emission measure $\phi(T)$ depends only on the continuum flux. Eq. (4), applied to the sulfur, calcium, and iron lines, gives the abundance of these elements with respect to hydrogen.

4. Results and discussion

4.1. Absolute abundances of S, Ca and Fe

The average S, Ca, and Fe abundances from each of the 57 flares are plotted as a function of flare number in Fig. 3. The vertical error bars represent the standard deviation of results from the individual spectra selected for that flare. The plots show a tightness of abundance results, with about a factor of two variability from flare to flare. The dashed line in each plot represents the accepted value of the photospheric elemental abundance from Grevesse & Anders (1989) for sulfur and calcium, and a more recent value of 3.2×10^{-5} for iron (Feldman 1992). The mean *Yohkoh* abundance of intermediate-FIP sulfur relative to hydrogen is $7.9 \pm 1.4 \times 10^{-6}$, smaller than the photospheric value by over a factor of two. The mean abundance of low-FIP calcium is $3.4 \pm 0.5 \times 10^{-6}$, about 50% greater than the photospheric value. The mean abundance of low-FIP iron shows greater scatter around its mean value of $4.5 \pm 1.3 \times 10^{-5}$, but is still about a factor of 1.4 higher than the accepted photospheric value.

This analysis depends on the accuracy of the determination of the thermal continuum. If there were an extra contribution to the recorded background, the thermal continuum emission would be lower, thus increasing the derived abundance value. The orbital background contribution is of the order of 0.05 counts/pixel/s and has a negligible contribution during flares. The contribution of continuum emission from other active regions can often be estimated from the pre-flare spectra. For calcium, it can be about 2 percent near the flare peak and less than 10 percent near the end of the flare. For sulfur this contribution can be up to 5–10 percent near the flare peak, and up to 20 percent near the flare end. Since we are analyzing simultaneous spectra of sulfur, calcium and iron, we use only that part of the flare which has good quality Fe XXV spectra. Fe XXV lines are emitted in hotter plasmas and their intensities decay faster than Ca XIX and S XV. Therefore, we do not use data from the far decay of flares and the active region contribution to the flare continuum in S XV has been assumed to be 10 percent for all flares. This only affects the abundance of sulfur, and the sulfur abundance values in Table 1 and Fig. 3 have been increased by 10 percent.

There are two other possible sources of a systematic error. The absolute sensitivities of all three channels are known to about 10 percent accuracy, which affects the Fe abundance and the relative S:Ca abundance. Also, systematic difference of up to 20 percent in theoretical calculations of the line emissivity can arise from different published calculations of the ionization balance.

4.2. Implications for the coronal abundance models

Abundances obtained in the previous section can be compared with the vast number of other spectroscopic and SEP measurements available in the literature. Fig. 4 shows a plot of coronal elemental abundances normalized to their photospheric values as a function of FIP. The dashed lines show the two empirical models: (1) low-FIP elements enhanced by a factor of four with

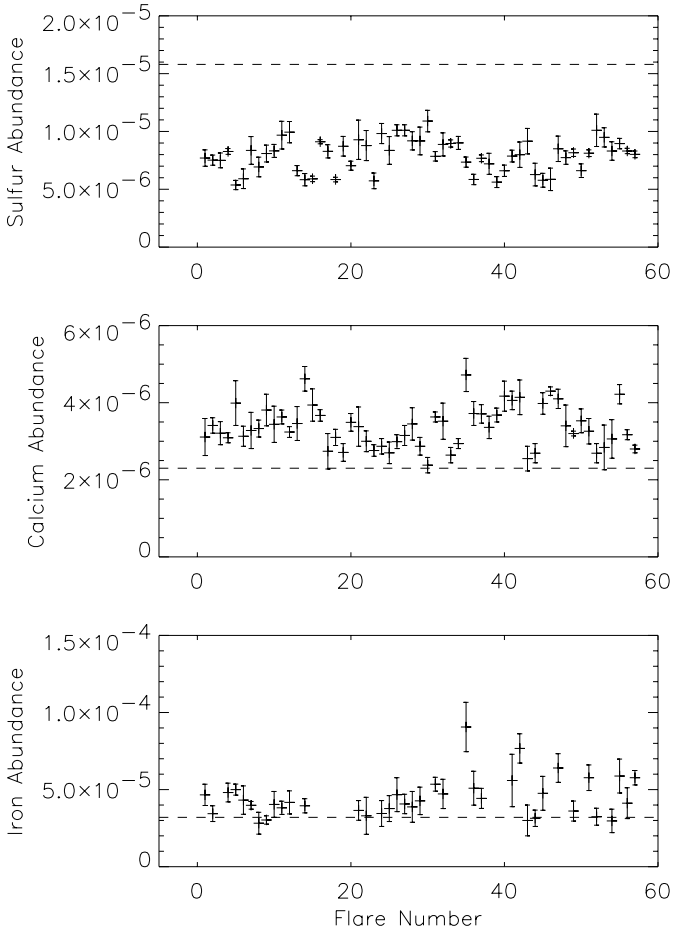

Fig. 3. The average abundance values of S, Ca, and Fe relative to H for the analyzed flares displayed as a function of a flare number: sulfur (*top panel*), calcium (*middle panel*), iron (*bottom panel*). Each data point corresponds to one flare. Dashed horizontal lines represent the photospheric abundances.

respect to their photospheric values and high-FIP elements the same in the corona and the photosphere (Feldman 1992; Meyer 1993); and (2) low-FIP elements the same in the corona and the photosphere and high-FIP elements depleted by a factor of four with respect to their photospheric values (Meyer 1985, 1991).

The data often used to support option (1) are the SEP results of Reames (1995). These data are from gradual events where the ambient coronal plasma is swept up by the expanding shock of a coronal mass ejection. These results are thought to be most closely associated with those of active region (closed loop) plasma and are depicted with the asterisks in Fig. 4. The diamonds depict normalized abundances of plasma from corotating interaction regions, i.e., results from material emerging from coronal holes (Reames 1995). As expected, both of these data sets show the enhancement of low FIP elements over their photospheric counterparts. However, it should be noted that none of these elements is enhanced by as much as a factor of four; moreover, the coronal abundances of all the high FIP elements are depleted.

The paper most often cited to support option (2) and to show that high FIP elemental abundances are depleted from their corresponding photospheric values is that by Veck & Parkinson (1981). While it is true that they find depletion of the high FIP element argon and intermediate FIP element sulfur, they also find a mean coronal Ca abundance value that is almost two times the photospheric value, (but with a large spread which could be interpreted as either uncertainty or abundance variations). The mean value is clearly not consistent with the photospheric value of Ca, as often implied.

All the other line-to-continuum measurements also fall in between the two model predictions: results by Sterling et al. (1993) (Ca only), several papers analyzing SMM spectra (Ca only), and the results of this paper (Ca, Fe, and S) are depicted in Fig. 4 with different symbols. All data show a depletion of high and intermediate FIP elements, but none by as much as a factor of four. In addition, the values for the low FIP elements are higher than photospheric. The highest Ca enhancement is found by Sylwester et al. (1998) who give examples of the Ca flare abundance variability as determined from line-to-continuum data from SMM. While their average Ca abundance is indeed enhanced over the photospheric value by a factor of 2.5, very few are enhanced by a factor as great as four.

In addition to the line-to-continuum measurements, there are several other areas of abundance research that do not agree with the simple model of enhancement of low FIP elements and photospheric values of high FIP elements. There have been multiple papers from authors claiming neon abundance variations in flares and active regions– from the SMM Gamma-Ray Spectrometer (Murphy et al. 1991; Share & Murphy 1995; Ramaty et al. 1995) and from the SMM Flat Crystal Spectrometer (Schmelz 1993; Schmelz et al. 1996). Such variations do not fit in with the simple scheme that abundances of high FIP elements are photospheric. There are additional results from Phillips et al. (1994, 1995) who analyze the K-alpha and K-beta lines of iron which suggest that there is an agreement to within a factor of 2 between the coronal and photospheric iron values. Finally, there are results from Raymond et al. (1997) using data from the Ultraviolet Coronagraph Spectrometer on the *Solar and Heliospheric Observatory* that show significant depletion of high FIP elements in streamers.

The spectroscopic and particle results agree that the abundances of low FIP elements are enhanced over their photospheric values, but not by as much as a factor of four. In addition, the abundances of high FIP elements are depleted, but also not by as much as a factor of four. Therefore, neither of the two standard empirical models represents faithfully the actual data. The weighted mean of all the low FIP coronal-to-photospheric values depicted in Fig. 4 (K-Si) is 2.1 ± 0.7 where 0.7 is the variance on the distribution of data points. The equivalent value for the high FIP elements (C-He) is 0.65 ± 0.22. There is clearly a spread in the distribution which is likely to result from something other than measurement error, and there is certainly abundance variability from one measurement to another.

Although Fig. 4 clearly shows that it is impossible to provide one model satisfying all observations, and although it is vi-

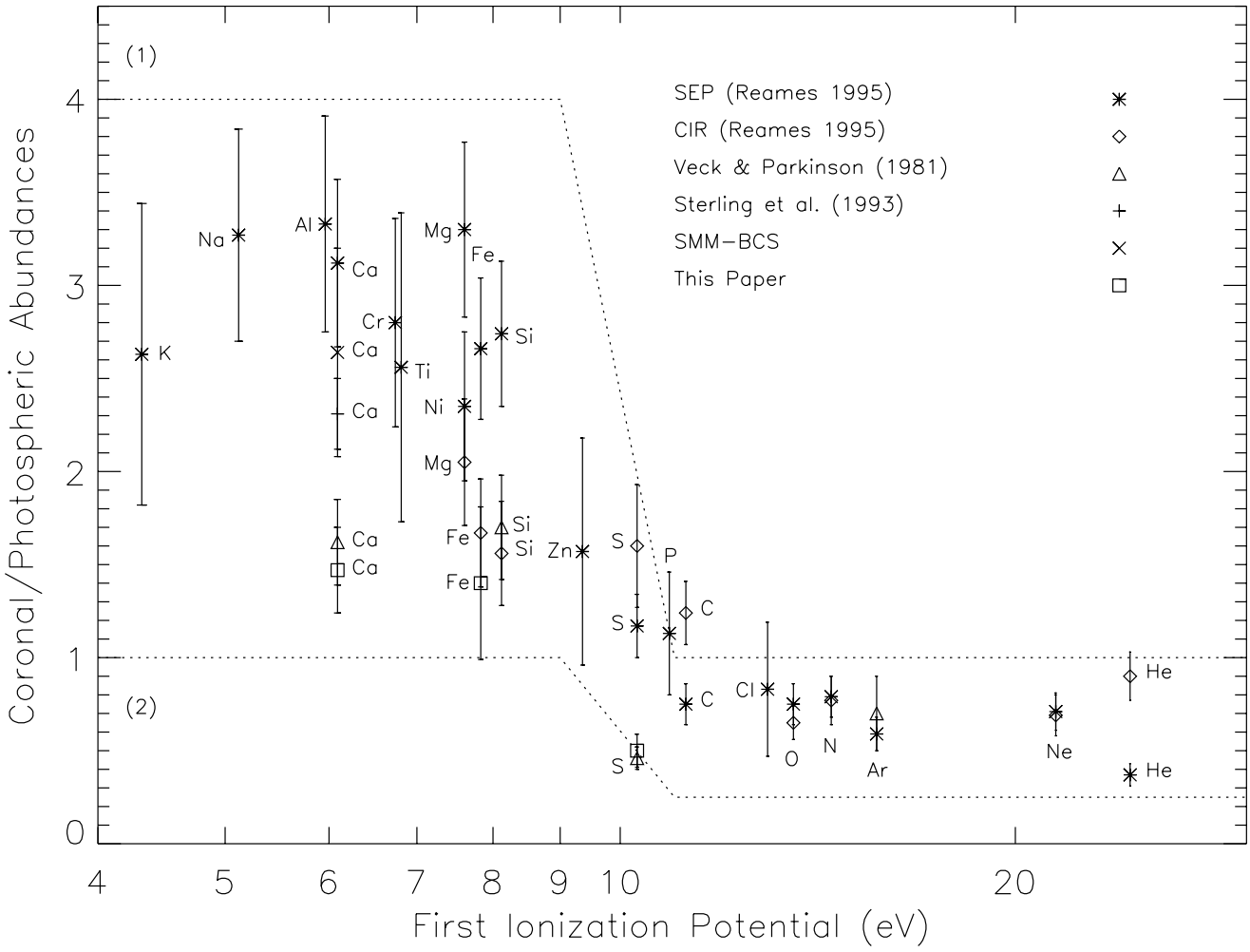

Fig. 4. Plot of coronal/photospheric elemental abundances as a function of FIP. The dashed lines represent the two empirical models (1) low-FIP abundance enhancement of a factor of four with respect to photospheric values or (2) high-FIP element depletion of a factor of four with respect to photospheric values. The data are from both interplanetary particle analysis and spectroscopy of closed coronal loops. Each data point represents many events – from 25 to several hundred – and the error bar depicts measurement uncertainty as well as statistically significant abundance variability.

tal to account for the possibility of abundance variability when analyzing any data set, it is also often useful to have a set of abundances to begin the analysis with. From the data analyzed here, it seems like this set should include both low FIP element enhancement as well as high FIP element depletion. The most probable set, called the hybrid abundances, is listed in Table 2. For comparison, we also list the abundances from Feldman et al. (1992 – model 1) which, according to the data in Fig. 4, set the normalization too high, as well as the "adopted coronal" abundances from Meyer (1985 – model 2) which set the normalization too low. The hybrid set of abundances seems to be a better representation of all the available data, but one must be careful to remember that abundances can certainly vary under different physical conditions, and not all data will agree precisely with a given normalization. If only one coronal abundance value were required for each element to represent an average of all spectroscopic and SEP observations, the hybrid abundances seem to represent the best we can do at this time. However, for individual data sets or classes of events, like the *Yohkoh* flare observations analyzed in this paper, the abundances derived directly from that particular data set should be used to ensure consistency with observations.

In summary, areas of research from several groups using various types of data from different instruments on numerous spacecraft have shown conclusively that the two step-like models are too simplistic to account for the complex abundance results described in the recent literature. We must now consider models that can deplete the abundance of high FIP elements as well as enhance the abundance of low FIP elements, and can no longer rely on a predetermined normalization for a set of abundances to understand a given spectroscopic data set.

5. Conclusions

For 57 flares observed with the BCS, we have used a DEM analysis using line and continuum fluxes to derive the coro-

Table 2. Coronal abundances from SEP and spectroscopic observations

Element	FIP (eV)	Photospheric Abundances	Coronal (1) Abundances	Coronal (1)/ Photospheric	Coronal (2) Abundances	Coronal (2)/ Photospheric	Hybrid Abundances	Hybrid/ Photospheric
K	4.32	1.33E-07					2.79E-07	2.10
Na	5.12	2.03E-06	8.51E-06	4.20	2.75E-06	1.36	4.25E-06	2.10
Al	5.96	3.00E-06	1.10E-05	3.65	2.75E-06	0.92	6.30E-06	2.10
Ca	6.09	2.16E-06	8.51E-06	3.94	2.94E-06	1.36	4.54E-06	2.10
Cr	6.74	4.77E-07					1.00E-06	2.10
Ti	6.81	8.47E-08					1.78E-07	2.10
Mg	7.61	3.78E-05	1.41E-04	3.74	3.73E-05	0.99	7.94E-05	2.10
Ni	7.61	1.74E-06	6.92E-06	3.98	2.16E-06	1.24	3.65E-06	2.10
Fe	7.83	3.21E-05	1.26E-04	3.92	3.92E-05	1.22	6.74E-05	2.10
Si	8.12	3.53E-05	1.26E-04	3.56	3.92E-05	1.11	7.42E-05	2.10
S	10.3	1.73E-05	1.86E-05	1.08	8.63E-06	0.50		
C	11.22	3.97E-04	3.89E-04	0.98	2.35E-04	0.59	2.57E-04	0.65
Cl	12.95	1.85E-07					1.20E-07	0.65
O	13.55	8.47E-04	7.76E-04	0.92	2.47E-04	0.29	5.48E-04	0.65
N	14.48	1.00E-04	1.00E-04	1.00	3.92E-05	0.39	6.47E-05	0.65
Ar	15.68	3.57E-06	3.80E-06	1.07	2.12E-06	0.59	2.31E-06	0.65
Ne	21.47	1.36E-04	1.20E-04	0.88	3.53E-05	0.26	8.83E-05	0.65
He	24.46	9.75E-02	7.94E-02	0.82	9.80E-02	1.01	6.31E-02	0.65

Photospheric abundances from Grevesse & Anders (1989)
Coronal (1) abundances from Feldman et al. (1992)
Coronal (2) abundances from Meyer (1985)
Hybrid abundances from the results depicted in Fig. 4 (see text)

nal abundances of sulfur, calcium, and iron. The mean *Yohkoh* abundance of intermediate-FIP sulfur relative to hydrogen is $7.9 \pm 1.4 \times 10^{-6}$, smaller than the photospheric value by over a factor of two. The mean abundance of low-FIP calcium is $3.4 \pm 0.5 \times 10^{-6}$, about 50% greater than the photospheric value. The mean abundance of low-FIP iron shows greater scatter around its mean value of $4.5 \pm 1.3 \times 10^{-5}$, but is still about a factor of 1.4 higher than the accepted photospheric value.

We find that neither of the standard empirical abundance models represents the BCS data correctly. In fact, they do not portray well the data they were created to represent. Elemental abundance values obtained from both interplanetary particle analysis and spectroscopy of closed coronal loops show low FIP elemental abundance enhancement by about a factor of two as well as high FIP elemental abundance depletion by roughly the same amount. An average value of all measurements (the hybrid abundances) are listed in Table 2. Excellent examples of abundance variability can be found in the literature so the values from Table 2 may not agree with all observations, but they do describe the best mean abundance values to date for coronal plasma.

Acknowledgements. *Yohkoh* is a mission of the Japanese Institute for Space and Astronautical Science. This work was supported by the United Kingdom PPARC and the NATO Collaborative Research Grant 910497. The authors thank University of Memphis physics students Henry Winter and Richard Scopes for help with data analysis. The authors also thank Drs John Raymond and Julia Saba for comments on the manuscript.

References

Arnaud M., Rothenflug R., 1985, ApJS 60, 425
Bely-Dubau F., Dubau J., Faucher P., Gabriel A.H., 1982a, MNRAS 198, 239
Bely-Dubau F., Dubau J., Faucher P., et al., 1982b, MNRAS 201, 1155
Dubau J., 1992, private communication
Culhane J.L., Bentley R.D., Hiei E., et al., 1991, Sol. Phys. 136, 89
Feldman U., 1992, Physica Scripta 46, 202
Feldman U., Mandelbaum P., Seely J.F., Doschek G.A., Gursky H., 1992, ApJS 81, 387
Fludra, A., Sylwester J., 1986, Sol. Phys. 105, 323
Fludra A., Schmelz J.T., 1995, ApJ 447, 936
Fludra A., Lemen J.R., Jakimiec J., Bentley R.D., Sylwester J., 1989, ApJ 344, 991
Fludra A., Bentley R.D., Culhane J.L., Lemen J.R., Sylwester J., 1991, Adv. Space Res. 11, (1)155
Fludra A., Culhane J.L., Bentley R.D., et al., 1993, Adv. Space Res. 13, (9)395
Fludra A., Doyle G., Metcalf T., et al., 1995, A&A 303, 914
Fludra A., Saba J.L.R., Henoux J-C., et al., 1999, Coronal Abundances. In: Strong K.T., Saba J.L.R, Haisch B.M., Schmelz J.T. (eds.) The Many Faces of the Sun. Springer-Verlag, p. 89
Grevesse N., Anders E., 1989. In: Waddington C.J. (ed.) Proc. AIP Conf. 183, Cosmic Abundances of Matter. Amer. Inst. of Physics, New York, p. 1
Lemen J.R., Phillips K.J.H., Cowan R.D., Hata J., Grant I.P., 1984, A&A 135, 313
Lemen J.R., Sylwester J., Bentley R.D., 1986, Adv. Space Res. 6, (6)245
McCann S.M., Keenan F.P., 1988, ApJ 328, 344
Meyer J.-P., 1985, ApJS 57, 173
Meyer J.-P., 1991, Adv. Space Res. 11, (1)269

Meyer J.-P., 1993, Adv. Space Res. 13, (9)377
Murphy R.J., Ramaty R., Kozlovsky B., Reames D.V., 1991, ApJ 371, 793
Phillips K.J.H., Pike C.D., Lang J., Watanabe T., Takahashi M., 1994, ApJ 435, 888
Phillips K.J.H., Pike C.D., Lang J., et al., 1995, Adv. Space Res. 15, (7)33
Ramaty R., Mandzhavidze N., Kozlovsky B., Murphy R., 1995, ApJ 455, L193
Raymond J.C., Kohl J.L., Noci G., et al., 1997, Sol. Phys. 175, 645
Reames D.V., 1995, Adv. Space Res. 15, (7)41
Schmelz J.T., 1993, ApJ 408, 373
Schmelz J.T., Saba J.L.R., Ghosh D., Strong K.T., 1996, ApJ 473, 519
Share G.H., Murphy R.J., 1995, ApJ 452, 933
Sterling A.C., Doschek G.A., Feldman U., 1993, ApJ 404, 394
Sylwester J., Lemen J.R., Mewe R., 1984, Nat 310, 665
Sylwester J., Lemen J.R., Bentley R.D., Fludra A., Zolcinski M.-C., 1998, ApJS 501, 397
Vainshtein L.A., Safronova U.I., 1978, Atomic Data & Nuclear Data 21, 49
Vainshtein L.A., Safronova U.I., 1985, Physica Scripta 31, 519
Veck N.J., Parkinson J.H., 1981, MNRAS 197, 41
Withbroe G.L., 1975, Sol. Phys. 45, 301